**TECHNICAL REPORT**
30 September 2022

For the project entitled:

**Mapping connectivity and conservation opportunity on agricultural lands across the conterminous United States: A species-agnostic approach**

Submitted to:

American Farmland Trust

**Background**

Preserving and enhancing the natural movement of organisms is critical to mitigating the current biodiversity crisis (Tilman et al. 2017) and is a key strategy for promoting species adaptations to climate change (Heller & Zavaleta 2009), with well-connected landscapes facilitating gene flow, migration, dispersal, and range shifts (McRae & Beier 2007; Littlefield et al. 2019). In the United States, private agricultural lands may play an important role in facilitating such ecological flows by providing linkages between areas of high-quality habitat (Kremen & Merenlender 2018; Garibaldi et al. 2021). Indeed, agricultural lands (including cropland, pasture, and rangeland) compose almost half the land area in the conterminous United States (CONUS) and, in many areas of the country, have continued to expand over the last decade (Lark et al. 2020). This trend is anticipated to continue (Sohl et al. 2014), underscoring the importance of centering agricultural landscapes in any comprehensive assessment of connectivity across the U.S.

Agricultural expansion, particularly high intensity crop production, has been a major driver of biodiversity declines globally through habitat loss, pesticide use, and the impacts of mowing and harvest (Newbold et al. 2015; Stanton et al. 2018). Intensively farmed areas may additionally represent substantial barriers to movement for a variety of taxa (Wimberly et al. 2018; Maas et al. 2021). However, low-intensity agriculture and wildlife-friendly management practices (e.g., grassland or forest strips, diversification of crops planted) can reduce these barriers to movement and even facilitate the flow of organisms across agricultural landscapes (Kremen & Merenlender 2018; Maas et al. 2021). Each year, governments spend billions of dollars globally to incentivize wildlife-friendly farming and other agri-environment schemes (Donald & Evans 2006), though limited information exists on where to target such financial incentives to maximize biodiversity benefits, potentially leading to the haphazard allocation of resources (Polasky et al. 2008; Kremen & Merenlender 2018).

Increases in global food production (of at least 25% by 2050; Hunter et al. 2017) will be necessary to support a growing human population. At the same time, climate change and urban and suburban expansion pose potential threats to food security by reducing the amount of land area that is highly suitable for cultivation (Tu et al. 2021; Kummu et al. 2021). It is therefore

imperative to balance the dual goals of promoting biodiversity and safeguarding the working lands that are most critical for food production (Leclère et al. 2020). Two general strategies have been proposed for balancing biodiversity and agricultural objectives: 'land sharing', i.e., maintaining or enhancing the capacity of cultivated lands to support biodiversity through wildlife-friendly farming practices, potentially at the expense of yield; and 'land sparing', which advocates intensifying food production in some areas while preventing the expansion of agriculture into more natural landscapes, e.g., through formal protection (Fischer et al. 2008; Phalan et al. 2011; Grass et al. 2019). The feasibility and desirability of land sharing vs. sparing will depend on local context (e.g., biophysical characteristics, land use history; Fischer et al. 2008) and at regional scales, elements of both strategies will be needed to maintain connectivity among protected areas and to support the flow of organisms that provide ecosystem services to agricultural lands (Kremen 2015; Grass et al. 2019; Garibaldi et al. 2021). Identifying which landscapes may be best suited to each strategy therefore represents a spatial conservation challenge. For instance, areas where both agricultural productivity and connectivity are high may provide key opportunities for incentive programs that promote both food production and the flow of organisms through wildlife-friendly farming practices. Alternatively, landscapes with high potential for long-term food production but relatively limited connectivity value may be good candidates for government programs that keep lands in production and protect against conversion to other land uses (e.g., urbanization).

To explore the importance of agricultural lands in supporting connectivity across the United States, we modeled potential net movement of organisms across all terrestrial landscapes in CONUS using a circuit theory-based connectivity modeling approach (McRae et al. 2008; Dickson et al. 2019). We then used our connectivity results and existing information on agricultural land quality across CONUS to identify conservation opportunities on agricultural lands that balance species connectivity and long-term food security. To facilitate use of these results by landowners, conservation advocates, and government agencies, we developed an interactive web map, which allows users to explore the novel spatial data generated by our analysis and provides guidance on using these layers to identify conservation opportunities.

**Methods**

To model connectivity across CONUS, we adopted an approach based on landscape structure, with less-modified landscapes assumed to support greater ecological flow (Dickson et al. 2017; Marrec et al. 2020). We tailored model parameters (e.g., maximum movement distances) to best reflect non-volant terrestrial vertebrates. Previous authors have noted that agricultural landscapes may represent 'invisible mosaics' (Fahrig et al. 2011), with a particular land cover category (e.g., cropland) actually representing a range of impacts on animal movement due to variation in management practices such as fertilizer application or cropping intensity. Here we build upon existing large-scale connectivity studies (e.g., McGuire et al. 2016; Dickson et al. 2017; Littlefield et al. 2017) by explicitly incorporating estimates of agricultural management intensity on cropland and pasture when determining landscape resistance to movement, using a novel method based on variation in vegetation cover during the growing season.

*Estimating human land use intensity*

To evaluate the influence that agricultural lands and other modified landscapes exert on ecological flow, we estimated human land use intensity (L) for all locations (i.e., pixels in a gridded landscape) across CONUS. Our estimates of human land use intensity were based on a procedure originally described by Theobald (2013), which assigns literature-supported values of intensity to multiple forms of human land use and integrates these values into a single spatial data layer ranging from 0 (unmodified, 'natural') to 1 (heavily modified). Similar human land use intensity layers have formed the basis of previous ecological flow-based connectivity models (e.g., Dickson et al. 2017; Marrec et al. 2020).

To quantify land use intensity on agricultural lands, we started with existing, static *L* estimates for individual agricultural cover types (Theobald 2013) and incorporated a dynamic measure of management intensity based on temporal variation in vegetation cover at a given location. We used high spatial resolution (10 m) data on 2016 land cover from American Farmland Trust's Farms Under Threat (FUT) analysis, which integrates data from multiple national-scale datasets to define several agricultural and non-agricultural cover classes (CSP 2020; data accessible from csp-fut.appspot.com). We focused on the four agricultural cover classes, which together account for 3.64 million km2, or approximately 47.6% of CONUS land area (Fig. 1). These agricultural

classes are cropland (1,549,077 km2 across CONUS), pasture (430,369 km2), rangeland (1,658,472 km2), and woodland (174,323 km2). The woodland class is a subset of the Natural Resources Inventory forest class defined as "natural or planted forested cover that is part of a functioning farm unit" and is no more than 160 m from cropland or pasture (CSP 2020). We assigned each of these four classes with a baseline value of land-use intensity (L) corresponding with the general level of human disturbance associated with that agricultural type. For cropland and pasture, baseline $L$ values of 0.5 and 0.4, respectively, were taken from Theobald (2013). Similar approaches to modeling ecological flow and/or landscape integrity have treated rangelands as having lower impact than cropland or pasture because rangelands tend to retain some natural vegetation cover and have relatively limited human influence (Buttrick et al. 2015; McRae et al. 2016). Woodlands are similarly characterized by relatively natural vegetation cover, albeit in close proximity to managed agricultural lands. We therefore assigned a baseline $L$ value of 0.2 to both rangelands and woodlands in an effort to capture the greater potential for wildlife movement through these cover types.
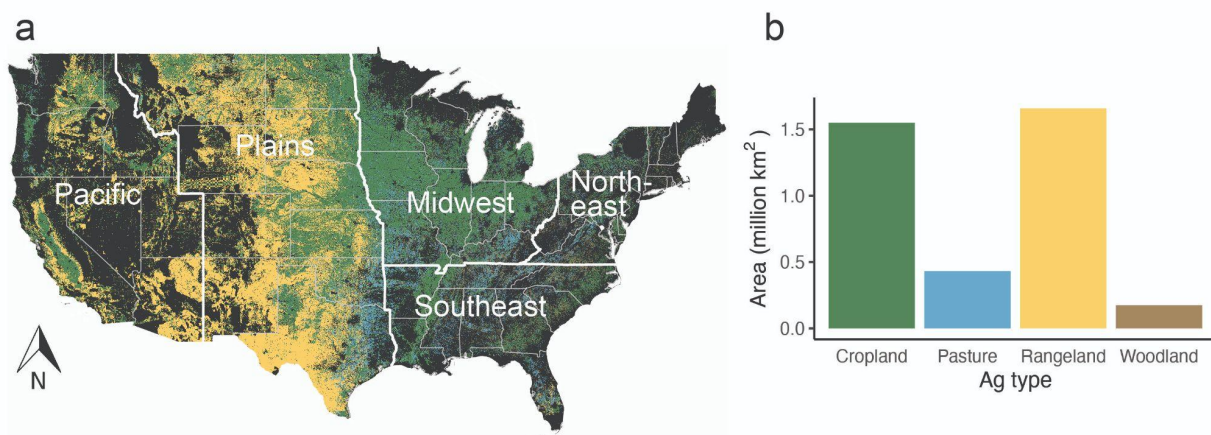


**Figure 1.** Agricultural land cover/use across the conterminous United States (CONUS). (**a**) Agricultural land cover is mapped across CONUS, with bold white lines and labels denoting Agricultural Research Service (ARS) regions. (**b**) Total area of each agriculture type across CONUS.

For both cropland and pasture, the agricultural cover types characterized by relatively intensive human management, we allowed $L$ values to vary between pixels of the same cover type based on estimates of management intensity. Management intensity estimates were derived from

temporal variability in vegetation cover based on the assumption that more intensively managed areas (e.g., croplands with high fertilizer inputs and/or multiple harvests per year; pasture subject to a high mowing frequency) will have greater variability in vegetation cover during the growing season than areas subject to less human intervention (e.g., fallow fields) (Franke et al. 2012; Gómez Giménez et al. 2017). We used a timeseries of Normalized Difference Vegetation Index (NDVI) values to estimate vegetation cover variability, acquiring cloud-free NDVI estimates at 16-day intervals from NASA's MODIS system (MOD13Q1 products). For each cropland and pasture pixel across CONUS, we used NDVI estimates over a five year period (2014-2018) centered on 2016, the year of our land cover dataset. NDVI estimates were acquired during the growing season for each year, with growing season start and end dates defined separately for each U.S. state based on the planting dates database developed by Sacks et al. (2010) (see Appendix A for details).

For each pixel of cropland and pasture, we calculated the coefficient of variation for all NDVI values across the time series (hereafter, cvNDVI) as our estimate of vegetation cover variability. The coefficient of variation was chosen to account for differences between vegetation types (e.g., different crops) and geographic location in average plant greenness. For each cover type (cropland or pasture), we centered cvNDVI values by first calculating the mean for all pixels of that cover type within the same USDA plant hardiness zone (PHZ; (USDA 2012)) and then subtracting this mean value from the value for each pixel. PHZs describe bands of average annual minimum winter temperature across CONUS. We centered cvNDVI values based on means within a PHZ to account for potential differences in vegetation cover variability across latitudes and climatic conditions (e.g., lower variability in areas with shorter growing seasons). Averages (± SD) of mean-centered cvNDVI were -0.05 (± 0.13) and -0.03 (± 0.10) for cropland and pasture, respectively. To derive the final $L$ value for cropland and pasture pixels, mean-centered cvNDVI values were added to the baseline $L$ value for each cover type (0.5 for cropland and 0.4 for pastureland, see above), resulting in a range of final $L$ estimates centered on the baseline value. Thus, pixels with lower than average vegetation cover variability for a given cover type and PHZ (i.e., negative mean-centered cvNDVI) received $L$ values below the baseline value for that cover type and those with higher than average variability (positive mean-centered cvNDVI) received $L$ values above the baseline. For rangeland and woodland, we did not

incorporate vegetation index data into $L$ estimates, instead using baseline $L$ values for all pixels under the assumption that variability in NDVI will be more strongly associated with phenology and plant community composition than with human management intensity in the cover types characterized by relatively natural vegetation.

We tested the validity of cvNDVI as a proxy for agricultural management intensity by comparing cvNDVI values between agricultural cover types; between irrigated, unirrigated, and fallow cropland; and across a gradient of nitrogen fertilizer use. These validation analyses are described in Appendix B. The validation steps confirmed the utility of cvNDVI as a proxy for management intensity, showing that (i) cropland pixels had significantly higher average cvNDVI than pasture; (ii) for both cropland and pasture, cvNDVI was positively correlated with nitrogen fertilizer usage; and (iii) among cropland pixels, irrigated crops had the highest average cvNDVI, followed by unirrigated crops and then fallow fields (Appendix B).

To create a comprehensive layer of human land use intensity across CONUS, we combined our novel agriculture $L$ layer with layers describing other forms of human land use, and incorporated the impact of nearby land uses and disturbances on a given location by allowing the value of each pixel to extend beyond the focal pixel itself. For all non-agricultural land uses we used an existing $L$ model (CSP 2019) that integrates multiple land use variables into three human impact categories - urban (including data on residential development and nighttime lights), transportation (including roads, railways, powerlines, and pipelines), and energy (including oil and gas wells, coal mines, and utility-scale solar and wind installations). Details on the development of the final $L$ layer ($L_{all}$) are provided in Appendix A.

*Estimating landscape resistance and modeling connectivity*

We used our final land use intensity layer, $L_{all}$, to derive a landscape resistance surface, which estimates the difficulty an organism experiences in moving through each pixel on the landscape (Zeller et al. 2012). Following Dickson et al. (2017), who conducted a sensitivity analysis to determine an appropriate formula for deriving resistance surfaces by rescaling $L$ values, we calculated resistance ($R$) as

$$R = (L_{all} + 1)^{10} + s/4,$$

where s is the percent slope of a given pixel, thus penalizing areas of steep slope to account for the effects of substantial elevational changes on the movement capacity of many terrestrial species (Dickson et al. 2017). This resulted in resistance values ranging between 1 (natural landscape) and 1032 (heavily modified landscape). We assigned all water bodies greater than approximately 100 m across a resistance value of 1000 to reflect the difficulty of moving through water for terrestrial species. The above rescaling formula led to a relatively high contrast between the resistance values assigned to locations with low, medium, and high $L_{all}$ values. For comparison, we derived a second resistance surface using a low-contrast rescaling formula suggested by Marrec et al. (2020). See Appendix C for a comparison of the two resistance surfaces and resulting connectivity models.

We modeled source strength, i.e., the predicted probability or intensity of movement from a given location on the landscape (McRae et al. 2008, 2016), as the degree of ecological intactness of a given pixel, which we calculated as 1 - $L_{all}$. Our source strength layer therefore ranged between 0 and 1, with relatively intact habitats receiving values close to 1, while partially modified landscapes (e.g., agricultural lands) received low but non-zero values. We assigned zero source strength to areas unlikely to represent sources of terrestrial animal movement, using the 2016 National Land Cover Data Base (NLCD; Dewitz 2019) to set pixels categorized as developed, open water, perennial snow/ice, or barren rock (i.e., all NLCD cover classes < 40) to zero. Resistance and source strength rasters for CONUS were derived at 250-m resolution using Google Earth Engine (GEE; Gorelick et al. 2017).

Following McRae et al. (2016), we ran omni-directional connectivity models across CONUS using the Omniscape algorithm. Omniscape is based on concepts from electronic circuit theory (McRae et al. 2008; Dickson et al. 2019), modeling the movement of organisms across the landscape as the flow of electrical current through a circuit. Omniscape allows users to fit "coreless" connectivity models in which every pixel may potentially serve as a source and/or target of movement, rather than only modeling connectivity between habitat cores, and thus allowing current to potentially flow in all directions. The algorithm uses a moving window

approach, iteratively treating every pixel in the source strength layer with a value greater than zero as a target for electrical current and connecting that pixel to all other non-zero pixels within the moving window radius, which serve as current sources. Current is then injected into the source pixels (with the amount of current proportional to source strength) and flows across the resistance surface (McRae et al. 2016; Landau et al. 2021). The cumulative current flow across all iterations of the moving window provides an estimate of the probability or intensity of the movement of organisms through every pixel on the landscape. The moving window radius is a key parameter, setting the maximum movement distance (i.e., the maximum distance between source and target pixels). Here we used a radius of 150 km, which approximates the upper dispersal distances of many large-bodied terrestrial vertebrates (Sutherland et al. 2000). To increase processing speed, we only treated every forty-first pixel as a (potential) target in the moving window. For comparison, we also ran connectivity models using smaller moving window radii, as described in Appendix C. Connectivity models were run in the Omniscape.jl software package in Julia (Landau et al. 2021).

We summarized cumulative current flow values from the Omniscape model within regions of the U.S. (defined by the USDA Agricultural Research Service [ARS]), and compared current flow on agricultural lands with that on other land cover/land use types (including developed and natural lands), providing an overview of agricultural land contributions to connectivity across the country. These analyses are described in detail in Appendix A. To further explore the drivers of high or low connectivity values on agricultural lands, we also estimate the total amount of natural land cover and development (based on NLCD categories) within a 1-km radius of each location on agricultural lands, hypothesizing that agriculture surrounded by greater amounts of natural land cover and lower levels of development would tend to have higher current flow. We tested the effect of surrounding land cover/land use on agricultural land current flow using a spatial error regression analysis (Dale & Fortin 2014) described in Appendix A.

*Identifying conservation opportunities on agricultural lands.*
To help identify and prioritize conservation opportunities on agricultural lands across CONUS, we categorized all agricultural pixels based on both their potential to support ecological flow and their value for long-term food production. This analysis drew upon results of the connectivity

model described above as well as a CONUS-wide data layer estimating productivity, versatility, and resilience (PVR; 10-m resolution) of agricultural lands circa 2016, which was developed as part of the FUT analysis described above (CSP 2020; viewable at csp-fut.appspot.com). PVR quantifies the long-term sustainability of maintaining a given area in cultivation based on soil and land cover characteristics and the type of agriculture practiced at a given location. See Appendix A for further details.

We masked the current flow and PVR datasets to only agricultural pixels and calculated quantiles of each dataset to identify pixels falling into 'low' (< 33% quantile), 'medium' (33% to 66%), and 'high' (> 66%) categories for connectivity and PVR. Because some regions have generally higher connectivity or PVR values than others, calculation of quantiles was conducted separately for each ARS region across CONUS. Thus, both connectivity and PVR values are considered relative to other agricultural pixels in the same region. We used these quantile estimates to generate a pixel-level bivariate map in which each pixel on agricultural land was ranked as 'low', 'medium', or 'high' for both connectivity and PVR. We used this map to link joint connectivity and food production value with specific conservation opportunities and/or financial incentives administered by the USDA.

**Results**

The importance of agricultural lands in facilitating the movement of organisms varied substantially across regions of the U.S. (Fig. 2, Table 1). At the ARS regional level, intensively cropped landscapes in the midwest (e.g., southern Minnesota, Iowa, and Illinois, Fig. 2) exhibited relatively high resistance to movement (Appendix D, Fig. D1) and low connectivity (Fig. 2, Table 1), while regions with extensive rangelands (e.g., central Nebraska, southwestern Texas) exhibited lower landscape resistance and were characterized by diffuse but relatively high current flow, comparable to natural landscapes in the western U.S. (e.g., central Nevada, northern Idaho; Fig. 2, Table 1). The plains region had the largest proportion of total land area in agriculture (70.0%) and, consequently, the greatest contribution of agricultural lands to overall connectivity in the region - agricultural lands accounted for 17.6% of top connectivity lands (i.e., lands in the top quartile of current flow, Appendix A) in the plains region (Table 1).
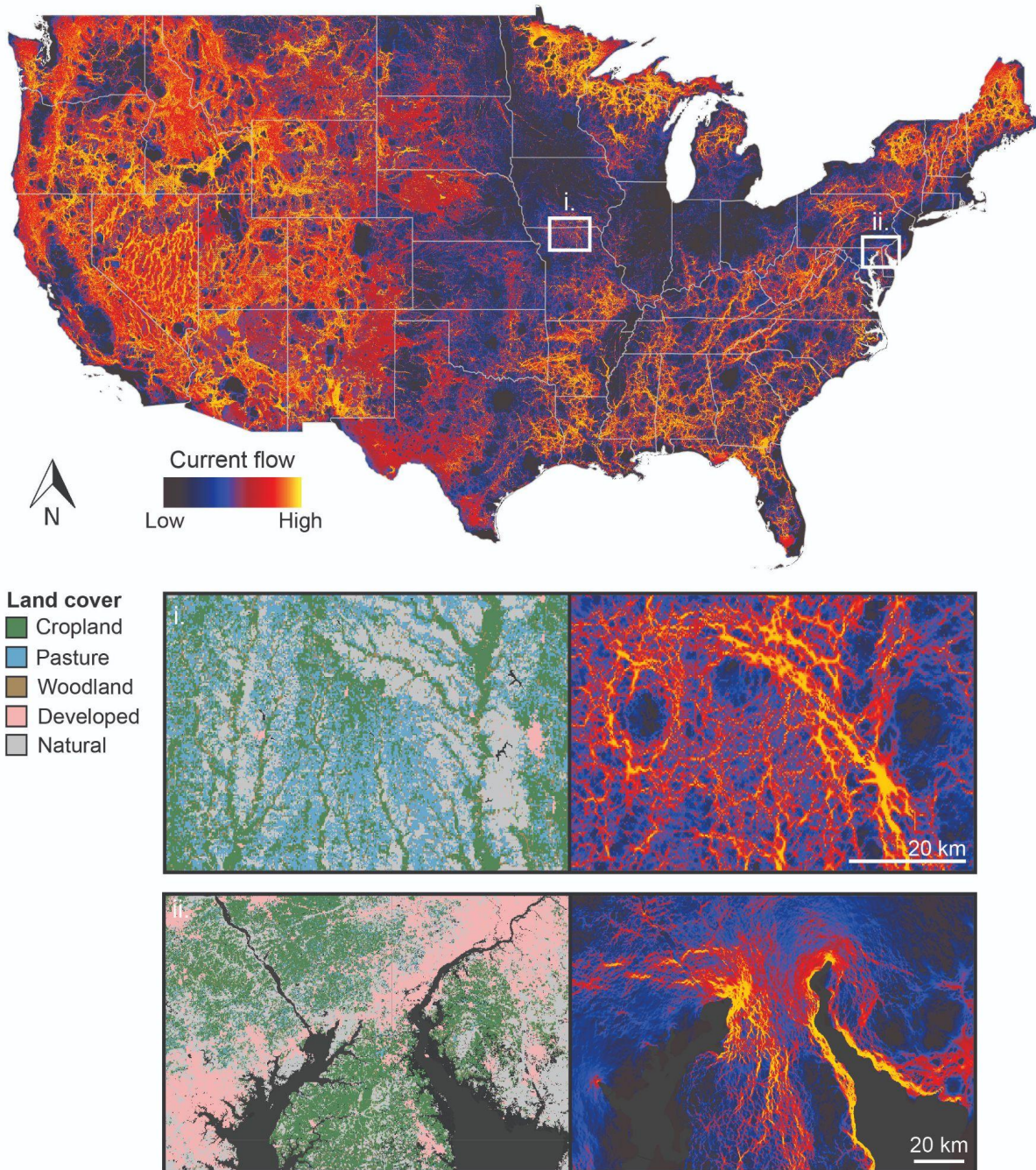
**Figure 2.** Map of connectivity (current flow) across the conterminous United States. Insets show details of agricultural landscapes with high connectivity value in (i) the central Midwest (northern Missouri) and (ii) the coastal Northeast (Delmarva peninsula, near the border of Maryland, Delaware, and Pennsylvania), where the persistence of patches of natural vegetation (forest fragments and strips of riparian or coastal vegetation) positively influence the current flow values of neighboring agricultural lands.

**Table 1.** Summary of connectivity on agricultural lands by Agricultural Research Service (ARS) region. *Percent in agriculture*: amount of total land area in the region categorized as cropland, pasture, rangeland, or woodland. *Current flow on agricultural lands*: mean (standard deviation) of current flow across all agricultural pixels in the region. *Agriculture contribution to top connectivity areas*: proportion of top lands for connectivity in the region (i.e., those with current flow values falling within the top quartile for the region) occurring on agricultural lands. ARS regions are shown in Fig. 1a.

| ARS region | Percent in agriculture | Current flow on agricultural lands | Agriculture contribution to top connectivity areas |
|---|---|---|---|
| Midwest | 51.2% | 92.0 (53.3) | 6.2% |
| Northeast | 21.1% | 116.1 (65.1) | 0.5% |
| Pacific | 29.5% | 160.2 (92.1) | 0.5% |
| Plains | 70.0% | 177.8 (93.0) | 17.6% |
| Southeast | 30.3% | 114.6 (70.2) | 1.2% |

Current flow on agricultural lands tended to be intermediate between current flow values of more developed landscapes (e.g., urban and suburban areas) and those of natural areas (including GAP 1 and 2 protected areas; Fig. 3a). The amount of natural and developed land in the vicinity of agricultural lands substantially influenced the connectivity value of individual agricultural pixels. Our top spatial error regression model (Table D1, $\Delta$AIC of next best model = 114.3) sufficiently accounted for spatial autocorrelation in model residuals (Moran's I = -0.03, p = 0.99) and included an interaction between agricultural cover type and the non-linear effects of surrounding land cover/use. Current flow values on all agriculture types were positively influenced by the amount of natural vegetation within 1 km (Fig. 3b, see also Fig. 2 insets) and negatively influenced by the amount of developed land within 1 km (Fig. 3c).

Mapping the combined rankings of current flow and PVR (Fig. 4) revealed that 2.7% of all agricultural lands (10.2 million hectares [Mha]) have high values for both connectivity and PVR (i.e., within the top 33% of agricultural lands in the same region; Table 2). The proportion of lands in this 'high-high' category varied between ARS regions, being lowest in the Plains (1.3%) and highest in the Northeast (5.8%, Table 2, Fig. 4 inset). Areas of low connectivity (i.e., values in the bottom 33%) and high PVR were more common overall, accounting for 21.3% of all

agricultural lands across CONUS (81.3 Mha), followed by areas of high connectivity and low PVR (15.5%, 59.3 Mha) and areas in the lowest category for both connectivity and PVR (4.2%, 16.2 Mha; Table 2).
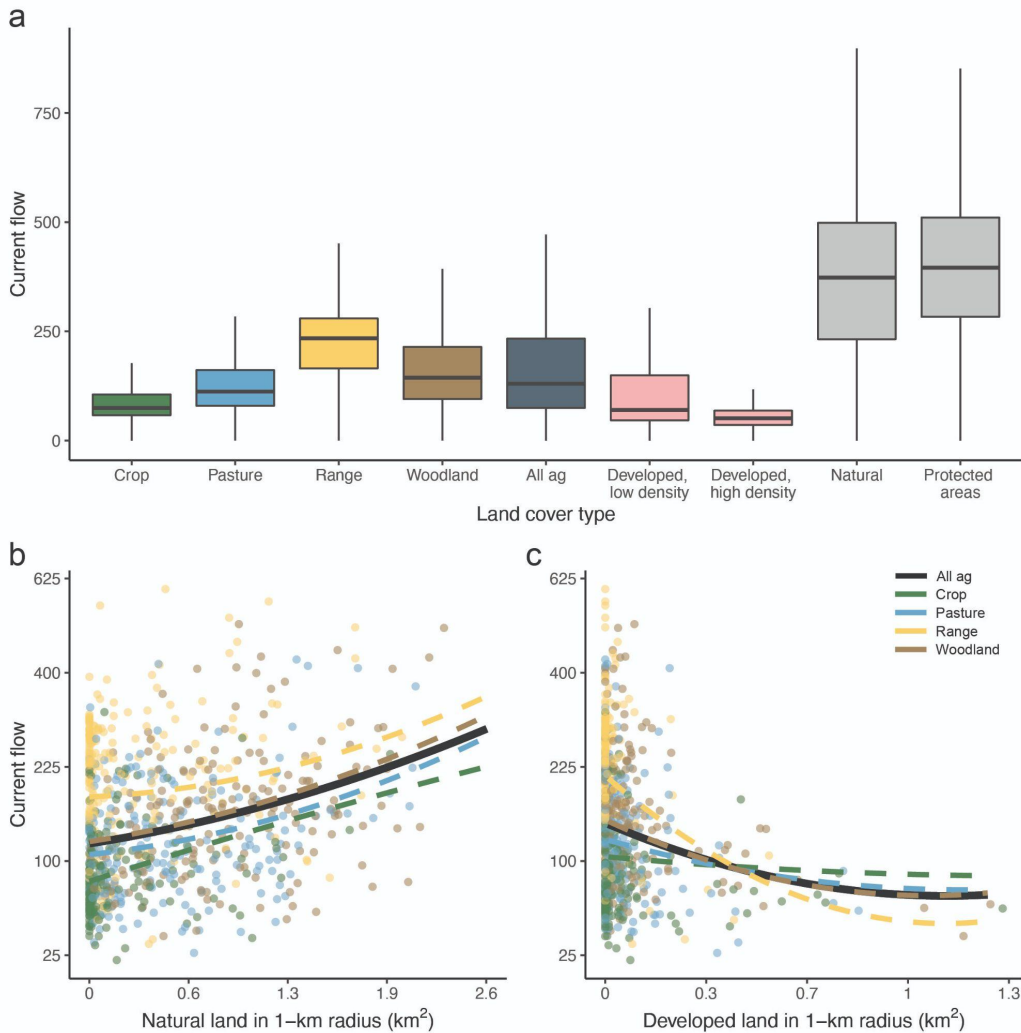


**Figure 3.** Current flow across land cover/use categories. (**a**) The range of current flow values on agricultural lands (cropland, pasture, rangeland, woodland, and all agricultural categories combined ['all ag']) is compared to that of developed areas and landscapes characterized by more natural land cover (i.e., all natural lands and lands within USGS GAP 1 and GAP 2 protected areas). Data are summarized as standard boxplots with whiskers representing 1.5 times the interquartile range. Outliers are excluded for clarity (see Appendix D, Figure D2 for a version with all outliers shown). Current flow values on agricultural land cover types are influenced by surrounding land cover/use, including the amount of (**b**) natural lands and (**c**) developed lands within 1 km. Fitted lines in **b** and **c** show the mean relationship between surrounding land cover and current flow as estimated by a spatial error model. For clarity, a randomly selected subset (n = 800) of data points used in the analysis are shown.
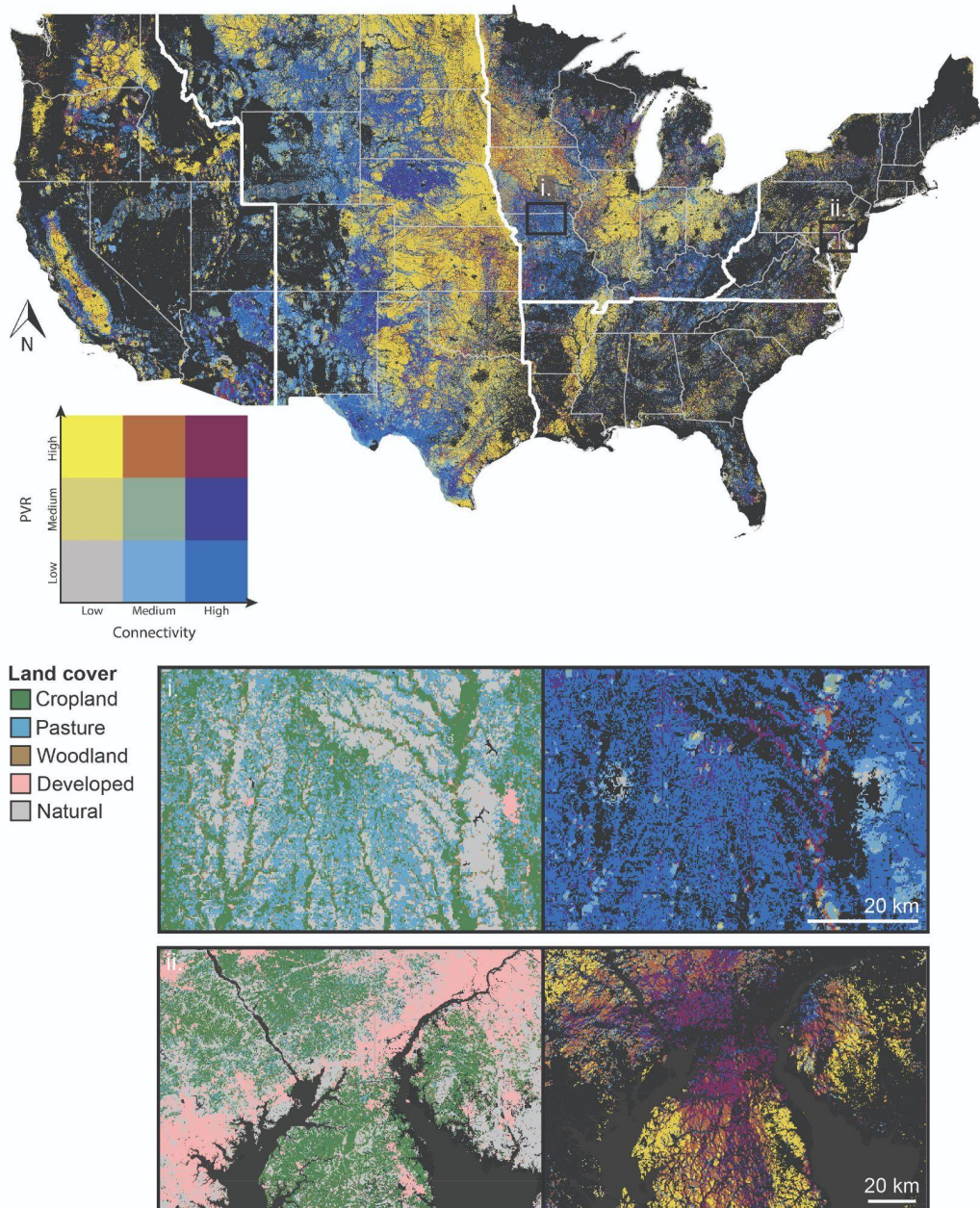
**Figure 4.** Map of agricultural lands ranked based on quantiles of connectivity (i.e., current flow) and productivity, versatility, and resilience (PVR), a measure of agricultural land quality. White lines indicate the boundaries of Agricultural Research Services (ARS) regions, within which quantiles of connectivity and PVR were calculated (color scales are therefore relative to other pixels in the same ARS region). Non-agricultural land cover/use types are shown in black. The insets show details of agricultural landscapes with high connectivity value and either high or low PVR, and correspond to those shown in Figure 2. The central Midwest landscape (i) is characterized by relatively high connectivity value but low PVR (deep blue color). The northern end of the Delmarva Peninsula (ii) has large amounts of land with high connectivity and high PVR (maroon color).

**Discussion**

Our results highlight the potential for agricultural lands across the U.S. to provide important movement routes for terrestrial species, supporting connectivity through otherwise heavily modified landscapes. Current flow through agricultural pixels depended strongly on the type of agriculture practiced at a given location and the intensity of human land use in the surrounding landscape. Generally, agricultural lands supported greater current flow than developed areas, suggesting an important role for agricultural lands as corridors linking areas of high-quality habitat. As the human footprint continues to expand, moderately impacted landscapes such as agricultural fields and grazing lands will be increasingly important movement habitat for many species (Suraci et al. 2020). Identifying conservation opportunities on agricultural lands is therefore critical to preventing further biodiversity loss while promoting long-term food security (Kremen & Merenlender 2018; Leclère et al. 2020).

Our maps reveal that landscapes ranking in the highest quantile for both connectivity and PVR constitute 10.2 Mha (approximately 3%) of agricultural lands across CONUS. These areas represent key opportunities for 'land-sharing' programs that promote biodiversity and food production on the same land holdings (Fischer et al. 2008, 2014; Kremen 2015; Garibaldi et al. 2021) by incentivizing wildlife-friendly farming practices (e.g., USDA's Conservation Stewardship Program and Environmental Quality Incentives Program [EQIP]) and protecting agricultural lands against conversion to more intensive land uses (e.g., USDA's Agricultural Conservation Easement Program [ACEP]). Increasing the capacity for farmland in this 'high connectivity-high PVR' category to support native species and wildlife movement - for instance, by planting non-crop vegetation strips along field edges and increasing crop diversity (Kremen et al. 2012) - may be critical for preserving connectivity in some areas of the U.S. and is consistent with recent proposals to increase conservation efforts on private lands (e.g., the Biden administration's commitment to conserve 30% of U.S. lands by 2030; Exec. Order No. 14008, 2021). Importantly, recent work has shown that incorporating such wildlife-friendly farming practices can stabilize (Gaudin et al. 2015) or even increase agricultural yields (Pywell et al. 2015), setting up the potential for biodiversity and food production 'win-wins' (Mitchell et al. 2013).

Our model results also identified substantial amounts of agricultural land across CONUS that are of high value for either connectivity (i.e., high connectivity-low PVR; 59.3 Mha in total) or food production (i.e., low connectivity-high PVR; 81.3 Mha) but not both. Such landscapes are particularly common in the Plains region, where large expanses of land with high PVR are devoted to intensive crop production (thus limiting connectivity value), but are interspersed with areas of less intensive agriculture on lower productivity lands. Such landscapes may be excellent candidates for a combination of management policies that reflect a 'land-sparing' conservation strategy (Phalan et al. 2011; Grass et al. 2019). Lands in the 'low connectivity-high PVR' category could be targeted for programs that keep lands in production and protect against conversion to development (e.g., ACEP), thus safeguarding the most productive agricultural lands. Meanwhile, neighboring areas in the 'high connectivity-low PVR' category could be maintained as low-intensity agriculture (pasture or rangelands) through enrollment in programs that support grazing (e.g., EQIP, CSP or USDA's term-limited Grasslands Conservation Reserve Program [CRP]) and/or through permanent easements (e.g., via ACEP). Where appropriate, such areas could also be considered for removal from production in favor of ecological restoration to support habitat and movement of native species (e.g., through USDA's Conservation Reserve Enhancement Program). Under such a conservation strategy, high-connectivity lands maintained as low-intensity agriculture or removed from agriculture altogether can act as connectivity 'stepping stones' (Wimberly et al. 2018; Doherty & Driscoll 2018) to support species movement through otherwise intensively managed landscapes and connect larger patches of high-quality habitat (e.g., protected areas). It is critical that any such land-sparing strategy be implemented at a relatively large spatial scale (i.e., across multiple land holdings within a region) to ensure sufficient connectivity across a network of 'spared' habitat patches to support dispersal and patch colonization and to prevent isolation of the larger protected areas that such habitat patches connect (Lamb et al. 2016; Grass et al. 2019). For more details on the amounts of land falling into each of the above described connectivity-PVR categories for all counties across the U.S., see Appendix E

Spatial context plays a substantial role in determining the connectivity value of agricultural lands. Our spatial regression analysis showed that, regardless of agriculture type, current flow on agricultural pixels was highest when those pixels were embedded in a broader landscape

consisting of large amounts of natural land cover. This finding is consistent with previous work showing that biodiversity in agricultural systems tends to be higher in heterogeneous landscapes consisting of a mix of agricultural and non-agricultural cover types (e.g., crop fields and pastures interspersed with woodlots and riparian buffers) (Donald & Evans 2006; Fahrig et al. 2011; Reynolds et al. 2018; Kremen & Merenlender 2018). By promoting connectivity, the presence of natural land cover in agricultural systems can also directly benefit food production, providing ecosystem services such as pollination and biological pest control through the (re)colonization and spillover of service-providing organisms from natural to cultivated patches (Blitzer et al. 2012; Kormann et al. 2016; Grass et al. 2019). Therefore, maintaining or restoring natural vegetation within agricultural systems is likely to have benefits across scales, promoting biodiversity and the provisioning of ecosystem services at the local level of individual farms while facilitating regional-scale connectivity across networks of working lands and protected areas.

Structural connectivity models such as the one used here are typically aimed at describing connectivity for a wide range of species (Dickson et al. 2017; Marrec et al. 2020) and perform well in terms of their overlap with focal species connectivity models, particularly for larger-bodied species or those with high movement capacity (Krosby et al. 2015). However, it is important to note that our model was not calibrated to the movement or habitat preferences of any particular focal species and thus may not fully capture the best movement pathways for a given species of interest. An important next step for connectivity conservation on agricultural lands will be to adapt the methods developed here in building connectivity models for focal species of conservation concern. Our NDVI-based approach to capturing variation in management intensity within a given agricultural cover type could readily be adapted to focal species functional connectivity models. Researchers can use species distribution models (Keeley et al. 2016) or resource selection functions (Zeller et al. 2014) to quantify the effect of agricultural management intensity on species habitat suitability or probability of use and translate these values into landscape resistance (Zeller et al. 2012; Suraci et al. 2020). Such efforts will be important for species-level management and will likely reveal substantial diversity in the capacity of agricultural lands to provide habitat value for individual species (Phalan et al. 2011; Reynolds et al. 2018).

We expect that our results will be useful in prioritizing conservation actions across a range of scales. At the local level, farmers, land trusts, and conservation advocates can use information on the joint value of agricultural lands for connectivity and food production to identify site-specific conservation strategies (e.g., land sparing vs. sharing), explore the types of conservation-focused financial incentives applicable to the landscapes they work in, and advocate for policies that support the conservation of working lands. At the state and federal levels, agencies tasked with administering agricultural conservation programs can use these results to better target funding to areas likely to have the greatest impact for promoting biodiversity and food security, ideally employing a landscape-scale approach that leads to heterogeneous agricultural-natural mosaics that benefit both producers and native species (Kremen et al. 2012). To help facilitate planning and conservation action based on our results, we have developed an interactive web application (https://cspbeta.z22.web.core.windows.net/), allowing users to visualize the spatial data developed here within their regions of interest. We hope that these tools can contribute to a collaborative process between landowners, governments, and conservationists to design landscapes that support both native species and a sustainable food supply.

## References

Blitzer EJ, Dormann CF, Holzschuh A, Klein A-M, Rand TA, Tscharntke T. 2012. Spillover of functionally important organisms between managed and natural habitats. Agriculture, Ecosystems & Environment 146:34–43.

Buttrick S, Popper K, Schindel M, McRae BH, Unnasch B, Jones A, Platt J. 2015. Conserving Nature's Stage: Identifying Resilient Terrestrial Landscapes in the Pacific Northwest. The Nature Conservancy, Portland, Oregon.

CSP. 2019. Methods and approach used to estimate the loss and fragmentation of natural lands in the conterminous U.S. from 2001 to 2017. Technical Report. Truckee, CA.

CSP. 2020. Description of the approach, data, and analytical methods used for the Farms Under Threat: State of the States project, version 2.0. Final Technical Report. Truckee, CA.

Dale MRT, Fortin M-J. 2014. Spatial Analysis: A Guide For Ecologists. Cambridge University Press.

Dewitz J. 2019. National Land Cover Database (NLCD) 2016 Products: U.S. Geological Survey

data release. Available from https://doi.org/10.5066/P96HHBIE.

Dickson BG et al. 2019. Circuit-theory applications to connectivity science and conservation. Conservation Biology 33:239–249.

Dickson BG, Albano CM, McRae BH, Anderson JJ, Theobald DM, Zachmann LJ, Sisk TD, Dombeck MP. 2017. Informing strategic efforts to expand and connect protected areas using a model of ecological flow, with application to the western United States. Conservation Letters 10:564–571.

Doherty TS, Driscoll DA. 2018. Coupling movement and landscape ecology for animal conservation in production landscapes. Proceedings of the Royal Society B: Biological Sciences 285:20172272. Royal Society.

Donald PF, Evans AD. 2006. Habitat connectivity and matrix restoration: the wider implications of agri-environment schemes. Journal of Applied Ecology 43:209–218.

Fahrig L, Baudry J, Brotons L, Burel FG, Crist TO, Fuller RJ, Sirami C, Siriwardena GM, Martin J-L. 2011. Functional landscape heterogeneity and animal biodiversity in agricultural landscapes. Ecology Letters 14:101–112.

Fischer J et al. 2008. Should Agricultural Policies Encourage Land Sparing or Wildlife-Friendly Farming? Frontiers in Ecology and the Environment 6:380–385. Ecological Society of America.

Fischer J, Abson DJ, Butsic V, Chappell MJ, Ekroos J, Hanspach J, Kuemmerle T, Smith HG, von Wehrden H. 2014. Land Sparing Versus Land Sharing: Moving Forward. Conservation Letters 7:149–157.

Franke J, Keuck V, Siegert F. 2012. Assessment of grassland use intensity by remote sensing to support conservation schemes. Journal for Nature Conservation 20:125–134.

Garibaldi LA et al. 2021. Working landscapes need at least 20% native habitat. Conservation Letters 14:e12773.

Gaudin ACM, Tolhurst TN, Ker AP, Janovicek K, Tortora C, Martin RC, Deen W. 2015. Increasing Crop Diversity Mitigates Weather Variations and Improves Yield Stability. PLOS ONE 10:e0113261. Public Library of Science.

Gómez Giménez M, de Jong R, Della Peruta R, Keller A, Schaepman ME. 2017. Determination of grassland use intensity based on multi-temporal remote sensing data and ecological indicators. Remote Sensing of Environment 198:126–139.

Gorelick N, Hancher M, Dixon M, Ilyushchenko S, Thau D, Moore R. 2017. Google Earth Engine: Planetary-scale geospatial analysis for everyone. Remote Sensing of Environment 202:18–27.

Grass I et al. 2019. Land-sharing/-sparing connectivity landscapes for ecosystem services and biodiversity conservation. People and Nature 1:262–272.

Heller NE, Zavaleta ES. 2009. Biodiversity management in the face of climate change: A review of 22 years of recommendations. Biological Conservation 142:14–32.

Hunter MC, Smith RG, Schipanski ME, Atwood LW, Mortensen DA. 2017. Agriculture in 2050: Recalibrating Targets for Sustainable Intensification. BioScience 67:386–391.

Keeley ATH, Beier P, Gagnon JW. 2016. Estimating landscape resistance from habitat suitability: effects of data source and nonlinearities. Landscape Ecology 31:2151–2162.

Kormann U, Scherber C, Tscharntke T, Klein N, Larbig M, Valente JJ, Hadley AS, Betts MG. 2016. Corridors restore animal-mediated pollination in fragmented tropical forest landscapes. Proceedings of the Royal Society B: Biological Sciences 283:20152347. Royal Society.

Kremen C. 2015. Reframing the land-sparing/land-sharing debate for biodiversity conservation. Annals of the New York Academy of Sciences 1355:52–76.

Kremen C, Iles A, Bacon C. 2012. Diversified Farming Systems: An Agroecological, Systems-based Alternative to Modern Industrial Agriculture. Ecology and Society 17. Available from https://www.readcube.com/articles/10.5751%2Fes-05103-170444 (accessed February 1, 2022).

Kremen C, Merenlender AM. 2018. Landscapes that work for biodiversity and people. Science 362. American Association for the Advancement of Science. Available from http://science.sciencemag.org/content/362/6412/eaau6020 (accessed August 5, 2021).

Krosby M et al. 2015. Focal species and landscape "naturalness" corridor models offer complementary approaches for connectivity conservation planning. Landscape Ecology 30:2121–2132.

Kummu M, Heino M, Taka M, Varis O, Viviroli D. 2021. Climate change risks pushing one-third of global food production outside the safe climatic space. One Earth 4:720–729. Elsevier.

Lamb A, Balmford A, Green RE, Phalan B. 2016. To what extent could edge effects and habitat fragmentation diminish the potential benefits of land sparing? Biological Conservation

195:264–271.

Landau VA, Shah VB, Anantharaman R, Hall KR. 2021. Omniscape.jl: Software to compute omnidirectional landscape connectivity. Journal of Open Source Software 6:2829.

Lark TJ, Spawn SA, Bougie M, Gibbs HK. 2020. Cropland expansion in the United States produces marginal yields at high costs to wildlife. Nature Communications 11:4295. Nature Publishing Group.

Leclère D et al. 2020. Bending the curve of terrestrial biodiversity needs an integrated strategy. Nature 585:551–556.

Littlefield CE, Krosby M, Michalak JL, Lawler JJ. 2019. Connectivity for species on the move: supporting climate-driven range shifts. Frontiers in Ecology and the Environment 17:270–278.

Littlefield CE, McRae BH, Michalak JL, Lawler JJ, Carroll C. 2017. Connecting today's climates to future climate analogs to facilitate movement of species under climate change. Conservation Biology 31:1397–1408.

Maas B, Brandl M, Hussain RI, Frank T, Zulka KP, Rabl D, Walcher R, Moser D. 2021. Functional traits driving pollinator and predator responses to newly established grassland strips in agricultural landscapes. Journal of Applied Ecology 58:1728–1737.

Marrec R, Abdel Moniem HE, Iravani M, Hricko B, Kariyeva J, Wagner HH. 2020. Conceptual framework and uncertainty analysis for large-scale, species-agnostic modelling of landscape connectivity across Alberta, Canada. Scientific Reports 10:6798. Nature Publishing Group.

McGuire JL, Lawler JJ, McRae BH, Nuñez TA, Theobald DM. 2016. Achieving climate connectivity in a fragmented landscape. Proceedings of the National Academy of Sciences 113:7195–7200. National Academy of Sciences.

McRae B, Popper K, Jones A, Schindel M, Buttrick S, Hall K, Unnasch R, Platt J. 2016. Conserving nature's stage: Mapping omnidirectional connectivity for resilient terrestrial landscapes in the Pacific Northwest. The Nature Conservancy, Portland, OR.

McRae BH, Beier P. 2007. Circuit theory predicts gene flow in plant and animal populations. Proceedings of the National Academy of Sciences 104:19885–19890. National Academy of Sciences.

McRae BH, Dickson BG, Keitt TH, Shah VB. 2008. Using circuit theory to model connectivity

in ecology, evolution, and conservation. Ecology 89:2712–2724.

Mitchell MGE, Bennett EM, Gonzalez A. 2013. Linking Landscape Connectivity and Ecosystem Service Provision: Current Knowledge and Research Gaps. Ecosystems 16:894–908.

Newbold T et al. 2015. Global effects of land use on local terrestrial biodiversity. Nature 520:45–50. Nature Publishing Group.

Phalan B, Onial M, Balmford A, Green RE. 2011. Reconciling Food Production and Biodiversity Conservation: Land Sharing and Land Sparing Compared. Science 333:1289–1291. American Association for the Advancement of Science.

Polasky S et al. 2008. Where to put things? Spatial land management to sustain biodiversity and economic returns. Biological Conservation 141:1505–1524.

Pywell RF, Heard MS, Woodcock BA, Hinsley S, Ridding L, Nowakowski M, Bullock JM. 2015. Wildlife-friendly farming increases crop yield: evidence for ecological intensification. Proceedings. Biological Sciences 282:20151740.

Reynolds C et al. 2018. Inconsistent effects of landscape heterogeneity and land-use on animal diversity in an agricultural mosaic: a multi-scale and multi-taxon investigation. Landscape Ecology 33:241–255.

Sacks WJ, Deryng D, Foley JA, Ramankutty N. 2010. Crop planting dates: an analysis of global patterns. Global Ecology and Biogeography 19:607–620.

Sohl TL et al. 2014. Spatially explicit modeling of 1992–2100 land cover and forest stand age for the conterminous United States. Ecological Applications 24:1015–1036.

Stanton RL, Morrissey CA, Clark RG. 2018. Analysis of trends and agricultural drivers of farmland bird declines in North America: A review. Agriculture, Ecosystems & Environment 254:244–254.

Suraci JP, Nickel BA, Wilmers CC. 2020. Fine-scale movement decisions by a large carnivore inform conservation planning in human-dominated landscapes. Landscape Ecology 35:1635–1649.

Sutherland GD, Harestad AS, Price K, Lertzman KP. 2000. Scaling of Natal Dispersal Distances in Terrestrial Birds and Mammals. Conservation Ecology 4. Resilience Alliance Inc. Available from https://www.jstor.org/stable/26271738 (accessed September 17, 2020).

Theobald DM. 2013. A general model to quantify ecological integrity for landscape assessments and US application. Landscape Ecology 28:1859–1874.

Tilman D, Clark M, Williams DR, Kimmel K, Polasky S, Packer C. 2017. Future threats to biodiversity and pathways to their prevention. Nature 546:73–81.

Tu Y, Chen B, Yu L, Xin Q, Gong P, Xu B. 2021. How does urban expansion interact with cropland loss? A comparison of 14 Chinese cities from 1980 to 2015. Landscape Ecology 36:243–263.

USDA. 2012. Plant Hardiness Zone Map. https://planthardiness.ars.usda.gov/. Available from https://planthardiness.ars.usda.gov/.

Wimberly MC, Narem DM, Bauman PJ, Carlson BT, Ahlering MA. 2018. Grassland connectivity in fragmented agricultural landscapes of the north-central United States. Biological Conservation 217:121–130.

Zeller KA, McGarigal K, Beier P, Cushman SA, Vickers TW, Boyce WM. 2014. Sensitivity of landscape resistance estimates based on point selection functions to scale and behavioral state: pumas as a case study. Landscape Ecology 29:541–557.

Zeller KA, McGarigal K, Whiteley AR. 2012. Estimating landscape resistance to movement: a review. Landscape Ecology 27:777–797.

**Appendix A. Supplementary methods**

*Defining growing season start and end dates for bounding NDVI time series data*

For each U.S. state, we used the planting dates database developed by Sacks et al. (2010) to extract the planting start date and harvest end date for a common crop type and used this as the date range within which NDVI estimates were acquired for all cropland and pasture pixels in that state. For consistency, we used corn as the crop type to define growing season dates for all states where corn is grown. For states where corn is not grown, we used another spring-planted crop represented in the database (spring barley in Nevada and potatoes in Maine, Massachusetts, and Rhode Island). For states that are absent from the database (Connecticut, Vermont, and New Hampshire), we used the planting start and harvest end dates for nearby states (in this case, other states in the New England region).

*Combining agricultural land use intensity with other human impacts*

To create a comprehensive layer of human land use intensity across CONUS, we combined our novel agriculture $L$ layer with an existing $L$ model (CSP 2019) that integrates multiple land use variables into three human impact categories - urban (including data on residential development and nighttime lights), transportation (including roads, railways, powerlines, and pipelines), and energy (including oil and gas wells, coal mines, and utility-scale solar and wind installations) - with each category stored as a separate raster layer. For full details on the existing $L$ layers, including dataset selection and assignment of land use intensity values, see CSP (2019). We combined these three layers with the new agriculture layer into a single land use intensity surface describing the impact at a given location ($L_{loc}$; ranging between 0 and 1) using the "fuzzy algebraic sum" (Theobald 2013). This algorithm ensured that the combined value for a given pixel was always at least as high as that of the most intense disturbance type, but that pixel values never exceeded 1. The fuzzy algebraic sum is given by

$$L_{loc} = 1 - \prod_{j=1}^{k} \left(1 - L_j\right),$$

where $L_j$ is the land use intensity for a given land use type $j$ (i.e., urban, transportation, energy, or agriculture), where $j = 1...k$ disturbance types (Theobald 2013).

Finally, we incorporated the impact of nearby land uses and disturbances on a given location (Ries et al. 2004) by allowing the value of each pixel in our $L_{loc}$ surface to extend beyond the focal pixel itself. We created a new surface of 'neighborhood' land use intensity, $L_n$, by allowing each pixel's $L_{loc}$ value to decay with distance, halving every 500 m out to a maximum distance of 10 km (Theobald et al. 2012; CSP 2019). We then combined $L_{loc}$ and $L_n$ to produce our final land use intensity layer ($L_{all}$), again using the fuzzy algebraic sum, i.e.,

$$L_{all} = 1 - ((1 - L_{loc}) * (1 - L_n)).$$

*Summarizing current flow values across regions and land cover/land use types*
We summarized cumulative current flow values from the Omniscape model within regions defined by the USDA Agricultural Research Service (ARS), providing an overview of large-scale differences in agricultural land contributions to connectivity across the country. We calculated the mean and standard deviation of current flow across all agricultural land pixels within each region and also estimated the overall importance of agricultural lands to connectivity in the region. For the latter, we first calculated the upper quartile (i.e., top 25%) value of current flow for all pixels in a given region, regardless of land cover/use type, and then calculated the proportion of those top current flow pixels that occurred on agricultural lands.

We compared current flow on agricultural lands with current flow on other land cover/land use types by first sampling current flow values at > 385,000 random points distributed across CONUS. We classified each random point as falling into one or more of the following categories: *cropland*, *pasture*, *rangeland*, *woodland*, or *all agriculture* (i.e., any one of the previous four categories), based on the FUT 2016 land cover layer (CSP 2020); *low density development,* based on the 2016 National Land Cover Data Base (NLCD; Dewitz 2019) (NLCD classes: 'developed, open space' and 'developed, low intensity' categories); *high density development* (NLCD classes: 'developed, medium intensity' and 'developed, high intensity' categories); *natural land cover* (all NLCD non-agricultural vegetation categories, i.e., cover

classes 41-74 and 90-95); and *protected areas* (all public lands in the USGS Protected Areas of the US Database v2.1(USGS 2020) categorized as GAP status 1 or 2, i.e., permanently protected and managed for natural land cover). Agricultural, developed, and natural land categories were mutually exclusive, and we gave preference to FUT agricultural land cover classes where these overlapped with low density development or natural lands. Other categories were non-exclusive; for instance, some natural land pixels were also in protected areas and vice versa. Random point sampling and extraction were conducted in GEE.

*Spatial error regression of the effect of surrounding land cover on agricultural land current flow*

To further explore the drivers of high or low connectivity values on agricultural lands, we also estimate the total amount of natural land cover and development (low and high density development categories combined) within a 1-km radius of each location on agricultural lands, hypothesizing that agricultural lands surrounded by greater amounts of natural land cover and lower levels of development would tend to have higher current flow. This was done for 40,000 randomly selected points on agricultural lands across CONUS (10,000 each for cropland, pasture, rangeland, and woodland). We tested the effect of surrounding land cover/land use on ag land current flow using spatial error regression (Dale & Fortin 2014), modeling current flow as a function of the amount of natural land within 1 km, the amount of developed land within 1 km, and second degree polynomial terms for amounts of natural and developed land to accommodate non-linearity in the response of current flow values to local land cover/use. We also fit a term for agricultural land cover type (categorical: crop, pasture, range, woodland) as well as terms for the interaction between agriculture type and the linear and polynomial effects of the amount of natural land and developed land within 1 km. All predictor variables were mean centered and continuous variables were scaled by one standard deviation prior to model fitting. Current flow values were square root transformed to normalize the spread of data. Prior to model fitting, we confirmed that there was limited correlation between continuous covariates (Pearson's correlation coefficient for amount of natural and developed land: $r = 0.11$). We defined spatial neighbors between the randomly sampled ag land points via Delauney triangulation and calculated a spatial weights matrix using row standardization (Bivand et al. 2013). We fit spatial error models using the simultaneous autoregression (SAR) approach (Dale & Fortin 2014) and

tested for remaining spatial autocorrelation in the SAR model using Moran's I. Spatial error models were fitted using the *spdep* and *spatialreg* packages in R (R Core Team 2021). In addition to a full model including all terms described above, we fit seven reduced models using subsets of the above terms as well as a null (intercept only) model (nine models total; see Appendix D, Table D1). We compared all models using a model selection approach and Akiake's Information Criterion (AIC; Burnham & Anderson 2002).

*Agricultural land productivity, versatility, and resilience (PVR)*

Agricultural land productivity, versatility, and resilience (PVR) is a CONUS-wide, 10-m resolution data layer describing the long-term sustainability of maintaining a given area in cultivation or other forms of production and is based on soil and land cover characteristics and the type of agriculture practiced at a given location circa 2016. Though technically a snapshot in time, PVR explicitly considers the potential for future disruptions of existing food production systems, thus identifying the "best" agricultural lands for long-term food security. Full details on the calculation of PVR are provided in the peer-reviewed technical documentation accompanying the Farms Under Threat analysis (CSP 2020). Briefly, PVR was calculated as the weighted sum of several (standardized) indicator layers representing soil productivity, land cover and use, food production for direct human consumption, and growing season length. The indicators included and their assigned weights were determined through formal expert elicitation in which 33 agriculture experts from across the U.S. participated in a structured process based on decision analysis theory (Saaty 2008). The values of the resulting PVR layer ranged between 0 and 1 (CSP 2020).

**Appendix B. Validating the relationship between vegetation index variability and management intensity**

Previous studies have found that time series of Normalized Difference Vegetation Index (NDVI) data are strongly related to management intensity in agricultural systems subject to frequent harvest/mowing and fertilizer inputs (Franke et al. 2012; Gómez Giménez et al. 2017). To test whether this relationship holds for agricultural lands across the conterminous U.S., we compared our NDVI coefficient of variation metric (cvNDVI, see main text) (1) between agricultural land cover types; (2) within a given land cover type across a gradient of nitrogen fertilizer input; and (3) between irrigated, unirrigated, and fallow cropland. We began by recalculating cvNDVI for a single year (rather than the five-year timespan used in the full analysis) to better match cvNDVI estimates to the particular crop type and fertilization and irrigation regimes used in a given year. For this validation analysis, we chose the year 2015 to match available fertilization and irrigation datasets (described below). We calculated 2015 cvNDVI for all agricultural cover types (not just cropland and pasture as in the full analysis) to allow comparison between cover types. For each of the four cover types, we randomly selected 20,000 locations across CONUS and extracted 2015 cvNDVI values at each point. For cropland and pasture points, we also extracted estimates of nitrogen fertilizer use in the year 2015 from a 5-km resolution layer developed by Cao et al. (2018). For cropland points, we extracted the crop type planted in 2015 based on the USDA's Cropland Data Layer (CDL) for that year, as well as a binary indicator of whether each cropland point was irrigated or not using a 30-m resolution dataset on irrigation extent across CONUS in the year 2015 (Xie & Lark 2021).

We visually compared the range of cvNDVI values between the four agricultural cover types using density plots, hypothesizing that cropland would exhibit a broader range of values than the other cover types given the potential for greater management intensity on croplands through irrigation, fertilization, multiple crop cycles, etc. Focusing on just cropland and pasture points, we used a spatial regression model (Dale and Fortin 2014) in an ANCOVA framework to test for effects of cover type (crop or pasture), amount of nitrogen fertilizer used, and their interaction on cvNDVI while accounting for spatial autocorrelation arising from proximity of randomly selected locations. Data on nitrogen fertilizer use were mean centered prior to model fitting. We

defined spatial neighbors between the randomly sampled points using Delauney triangulation and calculated a spatial weights matrix using row standardization (Bivand et al. 2013). We fit spatial error models using the simultaneous autoregression (SAR) approach (Dale & Fortin 2014) and tested for remaining spatial autocorrelation in the SAR model using Moran's I. Spatial error models were fitted using the *spdep* and *spatialreg* packages in R (R Core Team 2021).

Finally, examined the relationship between crop management intensity and cvNDVI for cropland points. For this analysis, we subsetted our dataset to just those cropland points that were planted as corn, soybeans, or wheat in 2015 (the three most common crop types in our dataset) or were left fallow, as determined by the 2015 CDL. We coded each point as falling into one of three management intensity categories - fallow, unirrigated crop, and irrigated crop - and again fit a spatial error model (using the procedure just described) testing the effect of cropland management intensity on cvNDVI. We compared means and 95% confidence interval (CI) values of cvNDVI from the spatial error model between each of the three management intensity categories.

We found that our estimate of vegetation cover variability (cvNDVI) performed well as a proxy for agricultural land management intensity. Across all randomly selected points, cropland, the cover type typically associated with the highest level of anthropogenic activity, had cvNDVI values that tended to be higher and more variable than those of all other agricultural cover types (Fig. B1).
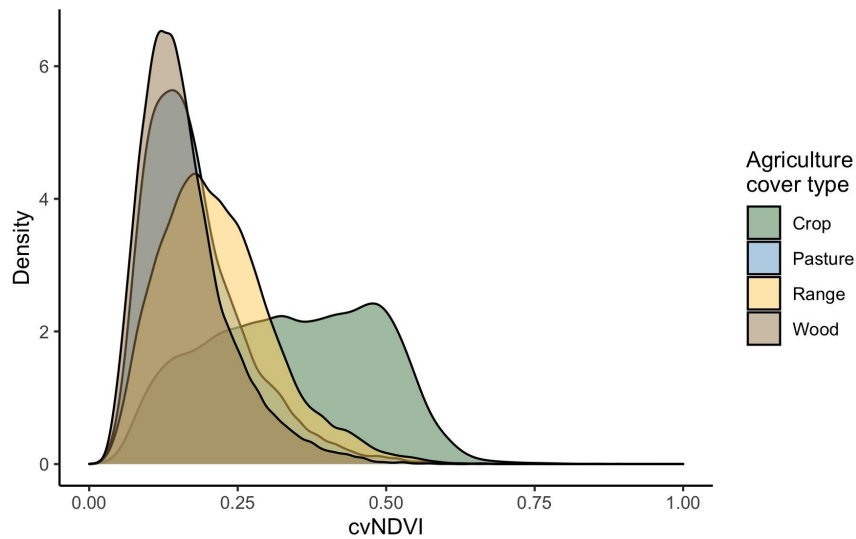
**Figure B1**. Density plot of the distribution of vegetation cover variability (estimated as the coefficient of variation of Normalized Difference Vegetation Index values, or cvNDVI) across all random points for each agricultural cover type.

The spatial error SAR model on nitrogen fertilizer and land cover type sufficiently accounted for spatial autocorrelation in the residuals (Moran's I = -0.05, $p$ = 0.99). The model revealed that cropland has on average a significantly higher cvNDVI than pasture and that, for both cover types, cvNDVI is positively related to nitrogen fertilizer usage but increases more quickly with fertilizer amount on cropland than on pasture (Fig. B2, Table B1).
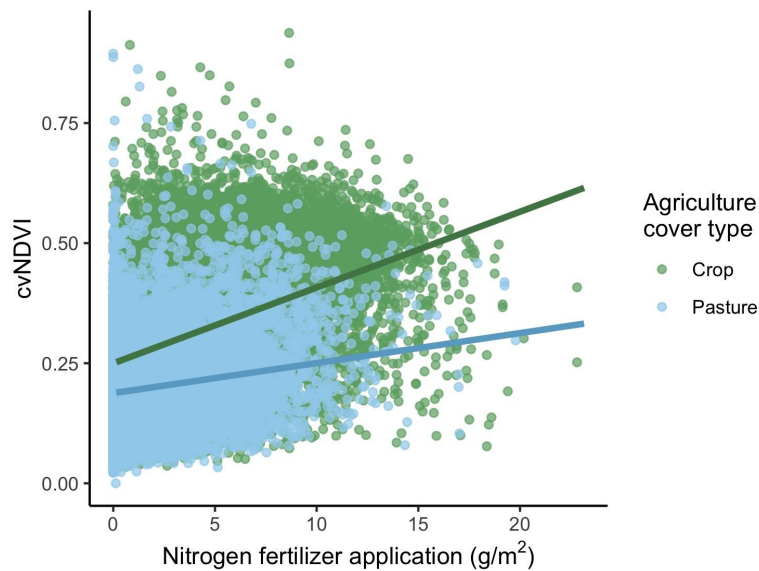
**Figure B2**. Relationship between nitrogen fertilizer usage and variation in vegetation cover (cvNDVI) on cropland (green) and pastureland (blue). Trend lines are fitted values from a spatial error regression model. For both agricultural cover types, increasing fertilizer usage is positively associated with cvNDVI, but with higher slope for cropland (Table B1).

**Table B1.** Spatial error regression analysis results for the effects of agricultural land cover type and nitrogen fertilizer use on variation in vegetation cover (cvNDVI).

|  | **Estimate** | **SE** | **P-value** |
|---|---|---|---|
| Intercept (Cover = Crop, Fertilizer = 0) | 0.2996 | 0.0013 | < 0.001 |
| Cover type (Pasture) | 0.0158 | 0.0003 | < 0.001 |
| Fertilizer | -0.0921 | 0.0011 | < 0.001 |
| Cover type x Fertilizer | -0.0095 | 0.0004 | < 0.001 |

The spatial error SAR model on cropland management intensity sufficiently accounted for spatial autocorrelation in the residuals (Moran's I = -0.07, $p = 0.99$) and revealed that more intensively managed cropland locations exhibited higher cvNDVI. Fallow fields had the lowest average cvNDVI, followed by unirrigated crops, with irrigated crops having the highest cvNDVI. Ninety-five percent confidence intervals, estimated by the spatial error model, did not overlap between management intensity categories (Fig. B3).
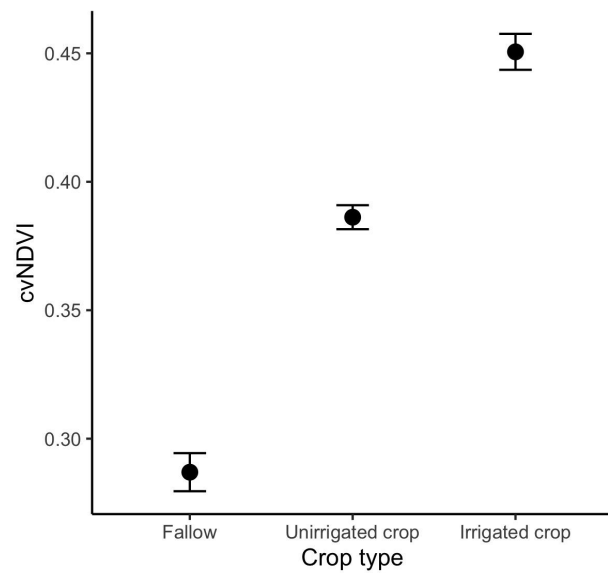
**Figure B3.** Mean (± 95% CI) values of vegetation cover variability (cvNDVI) for fallow agricultural fields, unirrigated crops, and irrigated crops. Means and CIs were calculated from a spatial error regression model.

**Appendix C. Sensitivity of connectivity model results to resistance surface scaling and moving window size.**

Connectivity model results are driven by the relative resistance values applied to different land cover types (Zeller et al. 2012). In the case of structural connectivity models based on estimates of the degree or intensity of human land use at each location across the study area, the scaling function used to convert land use intensity to resistance is therefore a key consideration. For the analyses presented in the main text, we followed Dickson et al. (2017) in calculating resistance ($R$) from human land use intensity ($L$) as

$$R = (L + 1)^{10} + s/4,$$

where $s$ is the percent slope of a given pixel (see main text for additional discussion and justification of this scaling function). The above rescaling formula led to a relatively high contrast between the resistance values assigned to locations with low, medium, and high $L$ values (Dickson et al. 2017). It was not our goal here to conduct a comprehensive sensitivity analysis of the effects of different scaling functions on resistance and connectivity; this analysis has already been conducted by Dickson et al. (2017) using a human land use intensity layer derived via very similar methods to those employed here. For comparison, however, we derived a second resistance surface using a low-contrast rescaling formula suggested by Marrec et al. (2020):

$$R = 1 + (1000 * L^2) + (s/4).$$

We then used this new, low-contrast resistance surface to fit a connectivity model in Omniscape, keeping all other model inputs and parameters (e.g., moving window radius, source strength surface) the same as those of the model presented in the main text.

The maximum distance between current flow start and end points is another key assumption of circuit theory-based connectivity models, controlled in Omniscape models by the radius of the moving window used to calculate current flow between source and target locations (McRae et al. 2016; Landau et al. 2021). In connectivity analyses focused on particular species or guilds, this

value is often set to the maximum (or average) movement or dispersal distance of that species or guild (e.g., Littlefield et al. 2017; Jennings et al. 2020). Here we were interested in modeling potential connectivity for a wide range of species as an estimate of ecological flow. We therefore chose to use a moving window radius comparable to the upper dispersal distances of many large-bodied terrestrial vertebrates (Sutherland et al. 2000) under the assumption that landscapes capable of supporting the movements of species with large space requirements will also support the movement of less vagile species. However, for comparison, we also fit connectivity models using two smaller moving window radii, (i) 20 km, comparable to the maximum dispersal distance of many medium sized mammals (Sutherland et al. 2000), and (ii) 5 km, approximating maximum dispersal distances for small vertebrates such as amphibians; (Marsh & Trenham 2001). For the connectivity models with smaller moving window radii, we kept all model inputs (i.e., resistance and source strength surfaces) the same as for the model presented in the main text, but varied the block size parameter to better match the moving window sizes used. Omniscape block size controls the density of pixels in a landscape raster that can potentially be treated as targets for current flow and can be used to decrease computation time with large landscape rasters (Landau et al. 2021). If block size = 1, all pixels are treated as potential targets (as long as source strength at the pixel is nonzero), with block size = 3, every third pixel is a potential target, and so on. We set block size to 21 for the 20-km model and 3 for the 5-km model. All models described here were based on 250-m resolution rasters.

To test the robustness of our conclusions regarding the relationship between current flow and land cover/use to model assumptions, we used the procedure described in the main text to extract current flow values for our primary connectivity model (i.e., the one presented in the main text) and for each of the three comparison models (i.e., the low-contrast, 20-km, and 5-km models) at > 385,000 random points distributed across the conterminous US (CONUS). Each point was assigned to one or more of the following land cover/use categories: cropland, pasture, rangeland, woodland, all agriculture, low density development, high density development, natural land cover, and protected areas (see main text for details). For each land cover/use category, we calculated Spearman's rank correlations ($\rho$) between current flow values from the primary model and those from each of the three comparison models. We also calculated the average current flow value for each land cover/use category under each model and compared the rank order of current

flow values across categories between the primary model and each of the comparison models using Spearman's rank correlations.

Correlation coefficients for each comparison are shown in Table C1 and suggest that model assumptions regarding the scaling function used to create the resistance surface and the size of the Omniscape moving window have relatively limited effects on the relationship between land cover/use and current flow. For all comparison models, land cover rankings were highly correlated with those of the primary model ($\rho \geq 0.99$). For individual land cover classes, current flow values derived from the primary model were typically strongly correlated with those derived from each of the three comparison models (Table C1), with the weakest correlations being for the high density development class with the 20-km ($\rho = 0.68$) and 5-km ($\rho = 0.59$) models.

**Table C1.** Spearman's rank correlations ($\rho$) between current flow values derived from the primary connectivity model (i.e., the model presented in the main text) and each of the three comparison models (described above) for each land cover/use category. The bottom row presents correlations for the rank order of average current flow values for each land cover/use category.

| Land cover/use category | Low-contrast scaling, $\rho$ | 20 km moving window, $\rho$ | 5 km moving window, $\rho$ |
|---|---|---|---|
| Cropland | 0.89 | 0.89 | 0.84 |
| Pasture | 0.93 | 0.91 | 0.86 |
| Rangeland | 0.92 | 0.88 | 0.80 |
| Woodland | 0.95 | 0.92 | 0.87 |
| All agriculture | 0.95 | 0.95 | 0.92 |
| Development, low density | 0.94 | 0.87 | 0.83 |
| Development, high density | 0.91 | 0.68 | 0.59 |
| Natural | 0.92 | 0.89 | 0.82 |
| Protected areas | 0.91 | 0.83 | 0.71 |
| *All categories, ranked* | 0.99 | 0.99 | 1.00 |

Finally, we mapped current flow across the CONUS for each of the three comparison models (Fig. C1), highlighting differences between models in the relative intensity and concentration of current flow. Current flow tended to be more diffuse in the 20-km and 5-km models relative to the low-contrast model (which used a 150-km moving window radius), reflecting the shorter movement distances allowed in the 20-km and 5-km models.
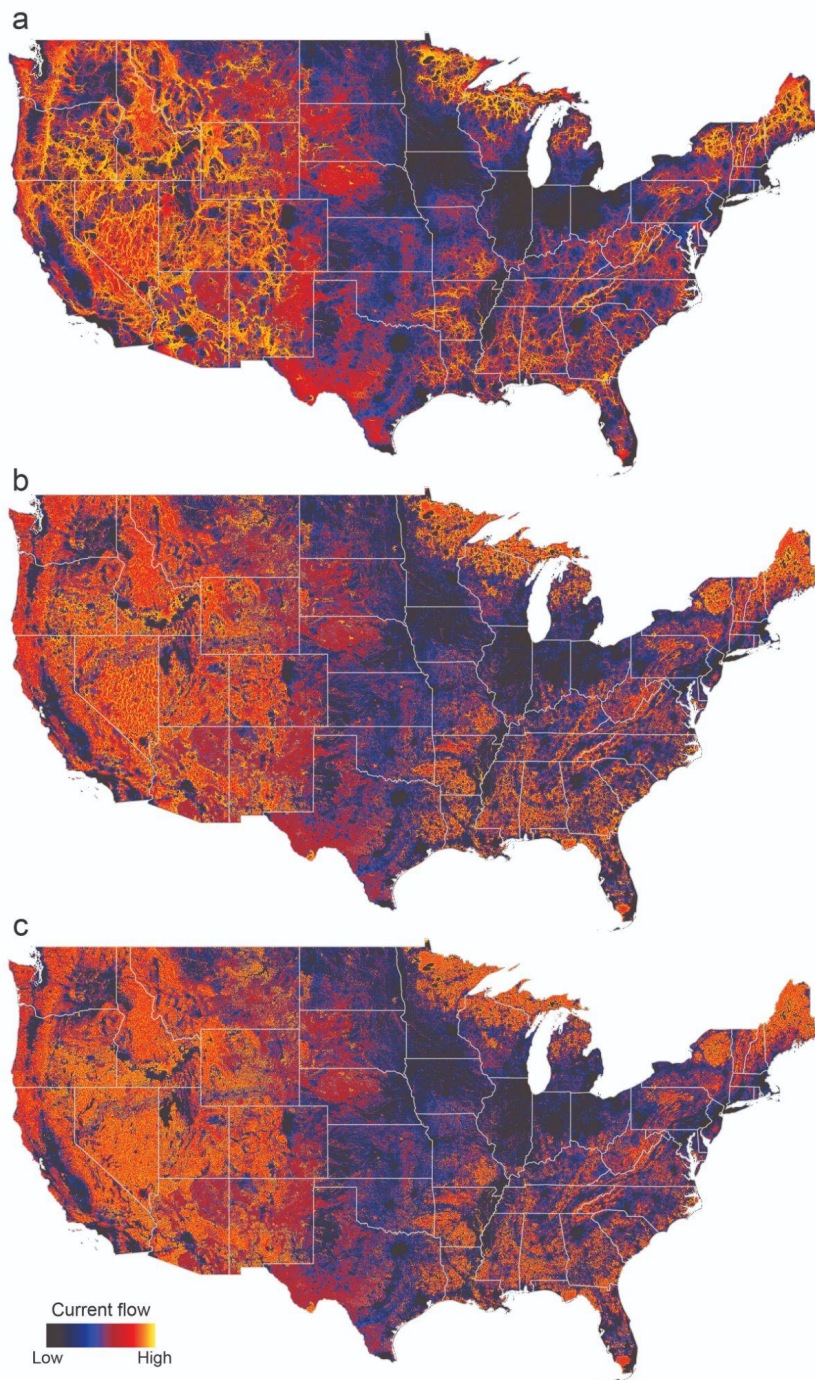


**Figure C1.** Current flow maps derived from each of the three comparison connectivity models described in Appendix B: (**a**) the low-contrast model, (**b**) the 20-km model, and (**c**) the 5-km model. Current flow is proportional to the potential net movement of organisms through a given location on the landscape.

# Appendix D. Supplementary tables and figures

**Table D1.** Model selection table for the spatial error regression model describing the effects of surrounding land cover/land use on agricultural land connectivity. The response variable in all models was the square root of current flow sampled at 40,000 random locations on agricultural lands across the conterminous United States. *nat* = amount of natural land within 1 km of the sampled location. *dev* = amount of developed land within 1 km of the sampled location. *ag type* = agricultural land cover class (cropland, pasture, rangeland, or woodland, as defined in the main text). Developed and natural land cover/use categories are based on the 2016 Nation Land Cover Database and defined in the main text.

| Model formula | Degrees of freedom | AIC | ΔAIC |
|---|---|---|---|
| nat + nat$^2$ + dev + dev$^2$ + ag type + nat * ag type + nat$^2$ * ag type + dev * ag type + dev$^2$ * ag type | 22.0 | 194303.3 | 0.0 |
| nat + dev + dev$^2$ + ag type + nat * ag type + dev * ag type + dev$^2$ * ag type | 18.0 | 194417.5 | 114.3 |
| nat + nat$^2$ + dev + dev$^2$ + ag type + dev * ag type + dev$^2$ * ag type | 16.0 | 194459.0 | 155.7 |
| nat + nat$^2$ + dev + dev$^2$ + ag type + nat * ag type + nat$^2$ * ag type | 16.0 | 194716.0 | 412.8 |
| nat + nat$^2$ + dev + ag type + nat * ag type + nat$^2$ * ag type + dev * ag type | 18.0 | 194738.0 | 434.7 |
| nat + dev + ag type + nat * ag type + dev * ag type | 14.0 | 194880.9 | 577.7 |
| nat + nat$^2$ + dev + dev$^2$ + ag type | 10.0 | 194935.2 | 632.0 |
| nat + dev + ag type | 8.0 | 195342.7 | 1039.5 |
| null model (~ 1) | 3.0 | 207905.0 | 13601.7 |

**Table D2.** Summary of landscape resistance and current flow values on agricultural lands (cropland, pasture, rangeland, and woodland, as well as all agricultural categories combined) compared to values in developed areas and natural landscapes. Developed and natural land cover/use categories are based on the 2016 Nation Land Cover Database and defined in the main text. Protected areas are USGS GAP 1 and 2 protected areas. Resistance and current flow values are presented as means (standard deviations).

| Land cover and use category | Resistance | Current flow |
|---|---|---|
| Cropland | 372.1 (202.1) | 91.1 (56.0) |
| Pasture | 217.9 (168.1) | 133.4 (84.4) |
| Rangeland | 65.1 (101.2) | 226.6 (92.9) |
| Woodland | 149.1 (152.3) | 169.6 (105.9) |
| All agriculture | 208.7 (211.2) | 158.8 (101.5) |
| Development, low density | 324.6 (247.6) | 131.2 (147) |
| Development, high density | 490 (202.5) | 59.5 (53.3) |
| Natural | 39.9 (112.3) | 378.5 (196.6) |
| Protected areas | 44.5 (161.7) | 401.2 (194.8) |
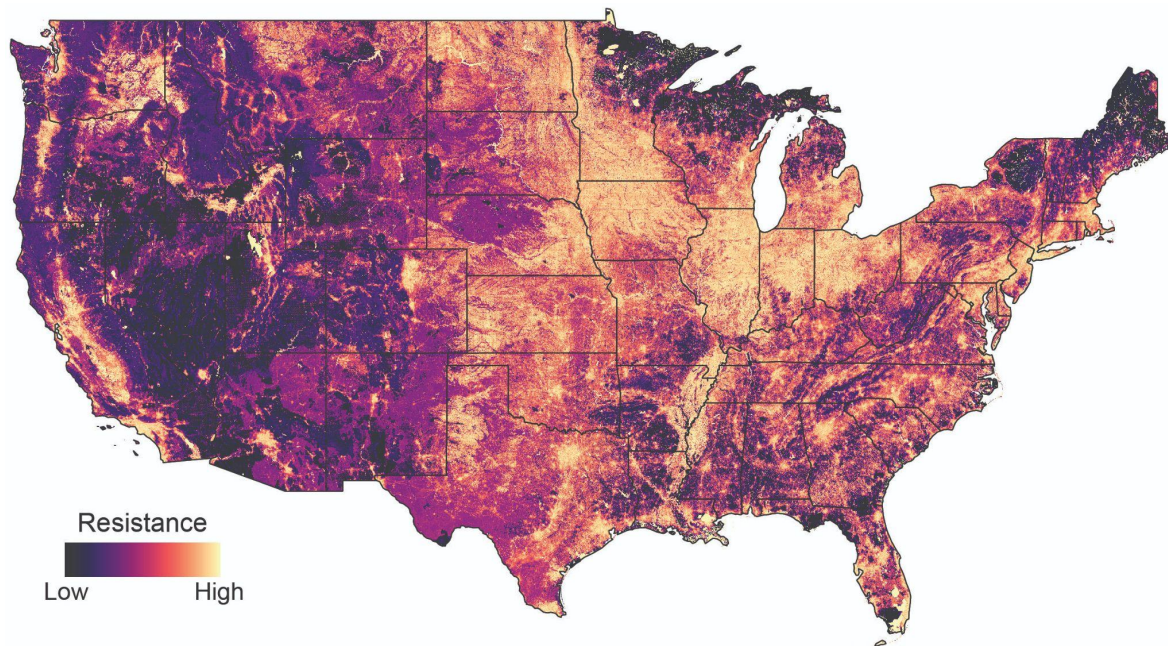


**Figure D1.** Map of landscape resistance across the conterminous United States
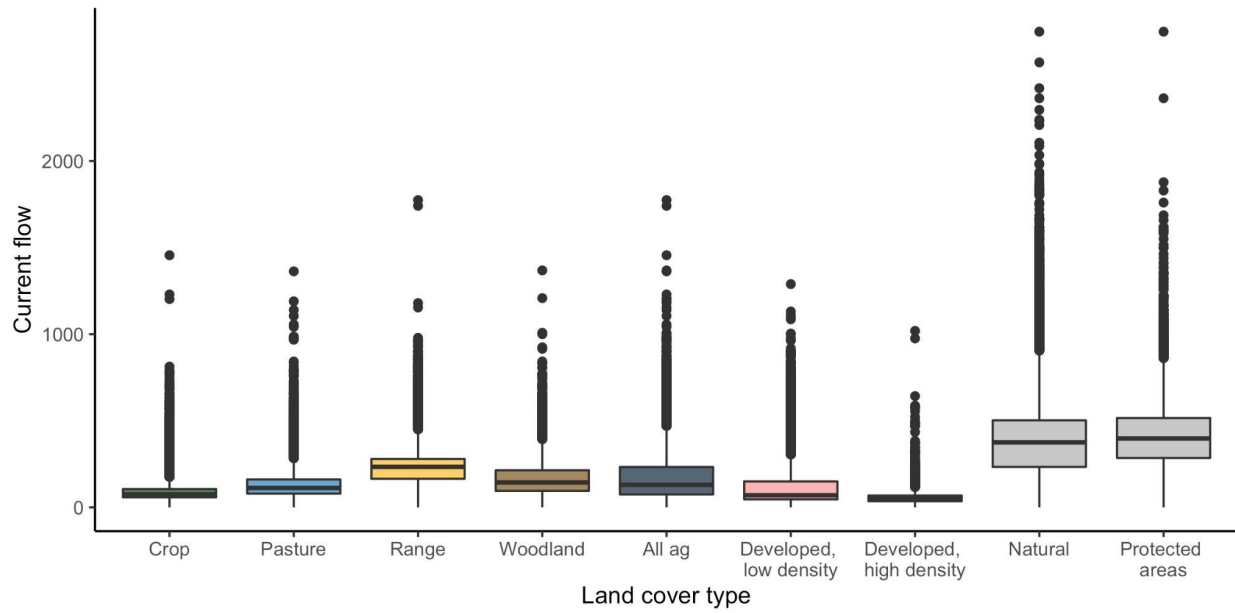
**Figure D2.** The range of current flow on agricultural lands (cropland, pasture, rangeland, and woodland, as well as all agricultural categories combined ['all ag']) is compared to that of developed areas and landscapes characterized by more natural land cover types (i.e., all natural lands and those within USGS GAP 1 or GAP 2 protected areas). Data are shown as standard boxplots with whiskers representing 1.5 times the interquartile range. Outliers are shown as points.

**Appendix E. Amount of land in each connectivity-PVR category by US county**

This data table (appended separately) quantifies the total number of acres of agricultural land in each county across the U.S. that fall into each of the key categories identified in our overlay analysis of connectivity value and productivity, versatility, and resilience (PVR) of agricultural lands (see main text and Figure 4 for more details). These categories are: (1) high value for connectivity with low PVR (coded *HH_acres* in the data table), (2) high connectivity with low PVR (*HL_acres*), (3) and low connectivity with high PVR (*LH_acres*). The total acres of agricultural lands in each county (*agAcres*) are also reported.

**References in appendices**

Bivand RS, Pebesma E, Gómez-Rubio V. 2013. Applied Spatial Data Analysis with RSecond. Springer, New York.

Burnham KP, Anderson DR. 2002. Model Selection and Multimodel Inference: A Practical Information-Theoretic Approach, 2nd edition. Springer, New York.

Cao P, Lu C, Yu Z. 2018. Historical nitrogen fertilizer use in agricultural ecosystems of the contiguous United States during 1850–2015: application rate, timing, and fertilizer types. Earth System Science Data **10**:969–984. Copernicus GmbH.

CSP. 2019. Methods and approach used to estimate the loss and fragmentation of natural lands in the conterminous U.S. from 2001 to 2017. Technical Report. Truckee, CA.

CSP. 2020. Description of the approach, data, and analytical methods used for the Farms Under Threat: State of the States project, version 2.0. Final Technical Report. Truckee, CA.

Dale MRT, Fortin M-J. 2014. Spatial Analysis: A Guide For Ecologists. Cambridge University Press.

Dewitz J. 2019. National Land Cover Database (NLCD) 2016 Products: U.S. Geological Survey data release. Available from https://doi.org/10.5066/P96HHBIE.

Dickson BG, Albano CM, McRae BH, Anderson JJ, Theobald DM, Zachmann LJ, Sisk TD, Dombeck MP. 2017. Informing strategic efforts to expand and connect protected areas using a model of ecological flow, with application to the western United States. Conservation Letters **10**:564–571.

Franke J, Keuck V, Siegert F. 2012. Assessment of grassland use intensity by remote sensing to support conservation schemes. Journal for Nature Conservation **20**:125–134.

Gómez Giménez M, de Jong R, Della Peruta R, Keller A, Schaepman ME. 2017. Determination of grassland use intensity based on multi-temporal remote sensing data and ecological indicators. Remote Sensing of Environment **198**:126–139.

Jennings MK, Zeller KA, Lewison RL. 2020. Supporting Adaptive Connectivity in Dynamic Landscapes. Land **9**:295. Multidisciplinary Digital Publishing Institute.

Landau VA, Shah VB, Anantharaman R, Hall KR. 2021. Omniscape.jl: Software to compute omnidirectional landscape connectivity. Journal of Open Source Software **6**:2829.

Littlefield CE, McRae BH, Michalak JL, Lawler JJ, Carroll C. 2017. Connecting today's climates to future climate analogs to facilitate movement of species under climate

change. Conservation Biology **31**:1397–1408.

Marrec R, Abdel Moniem HE, Iravani M, Hricko B, Kariyeva J, Wagner HH. 2020. Conceptual framework and uncertainty analysis for large-scale, species-agnostic modelling of landscape connectivity across Alberta, Canada. Scientific Reports **10**:6798. Nature Publishing Group.

Marsh DM, Trenham PC. 2001. Metapopulation Dynamics and Amphibian Conservation. Conservation Biology **15**:40–49.

McRae B, Popper K, Jones A, Schindel M, Buttrick S, Hall K, Unnasch R, Platt J. 2016. Conserving nature's stage: Mapping omnidirectional connectivity for resilient terrestrial landscapes in the Pacific Northwest. The Nature Conservancy, Portland, OR.

R Core Team. 2021. R: A language and environment for statistical computing. R Foundation for Statistical Computing, Vienna, Austria. Available from https://www.R-project.org/.

Ries L, Fletcher RJ, Battin J, Sisk TD. 2004. Ecological responses to habitat edges: Mechanisms, models, and variability explained. Annual Review of Ecology, Evolution, and Systematics **35**:491–522. Annual Reviews.

Saaty TL. 2008. Decision making with the analytic hierarchy process. International Journal of Services Sciences **1**:83–98. Inderscience Publishers.

Sacks WJ, Deryng D, Foley JA, Ramankutty N. 2010. Crop planting dates: an analysis of global patterns. Global Ecology and Biogeography **19**:607–620.

Sutherland GD, Harestad AS, Price K, Lertzman KP. 2000. Scaling of Natal Dispersal Distances in Terrestrial Birds and Mammals. Conservation Ecology **4**. Resilience Alliance Inc. Available from https://www.jstor.org/stable/26271738 (accessed September 17, 2020).

Theobald DM, Reed SE, Fields K, Soulé M. 2012. Connecting natural landscapes using a landscape permeability model to prioritize conservation activities in the United States. Conservation Letters **5**:123–133.

USGS. 2020. U.S Geological Survey (USGS) Gap Analysis Project (GAP). Protected Areas Database of the United States (PAD-US) 2.1: U.S. Geological Survey data release. Available from https://doi.org/10.5066/P92QM3NT.

Xie Y, Lark TJ. 2021. Mapping annual irrigation from Landsat imagery and environmental variables across the conterminous United States. Remote Sensing of Environment **260**:112445.

Zeller KA, McGarigal K, Whiteley AR. 2012. Estimating landscape resistance to movement: a review. Landscape Ecology **27**:777–797.